



# CHORUS

This is the accepted manuscript made available via CHORUS. The article has been published as:

## Improved pseudopotential transferability for magnetic and electronic properties of binary manganese oxides from DFT+U+J calculations

Jin Soo Lim, Diomedes Saldana-Greco, and Andrew M. Rappe

Phys. Rev. B **94**, 165151 — Published 21 October 2016

DOI: [10.1103/PhysRevB.94.165151](https://doi.org/10.1103/PhysRevB.94.165151)

1 **Improved Pseudopotential Transferability for Magnetic and**  
2 **Electronic Properties of Binary Manganese Oxides from**  
3 **DFT+ $U$ + $J$  Calculations**

4 Jin Soo Lim, Diomedes Saldana-Greco, and Andrew M. Rappe

5 *The Makineni Theoretical Laboratories,*

6 *Department of Chemistry,*

7 *University of Pennsylvania,*

8 *Philadelphia, PA 19104-6323, USA*

9  
10 (Dated: September 6, 2016)

11 **Abstract**

12 We employ the fully anisotropic DFT+ $U$ + $J$  approach with the PBEsol functional to investigate  
13 ground-state magnetic and electronic properties of bulk binary manganese oxides: MnO, Mn<sub>3</sub>O<sub>4</sub>,  
14  $\alpha$ -Mn<sub>2</sub>O<sub>3</sub>, and  $\beta$ -MnO<sub>2</sub>, in order of increasing Mn valence. The computed crystal structures,  
15 noncollinear magnetic ground states, and corresponding electronic structures are in good agreement  
16 with the experimental data and hybrid functional calculations available in the literature. We take  
17 into account the nonlinear core-valence interaction in our Mn pseudopotential designed by ourselves,  
18 as it has been proven to be important for transition metal systems. Although the Hubbard  $U$  term  
19 is capable by itself of opening a band gap, the explicitly defined exchange parameter  $J$  plays an  
20 important role in improving the detailed electronic and noncollinear magnetic structure profiles.  
21 Appropriate band gaps are obtained with  $U$  values smaller than those used in previously reported  
22 calculations. Our results suggest that pseudopotential design together with DFT+ $U$ + $J$  enables  
23 the acquisition of accurate properties of complex magnetic systems using a non-hybrid density  
24 functional.

## I. INTRODUCTION

Due to the low cost, low toxicity, and high chemical stability, binary manganese oxides have a wide range of applications, such as catalysis [1], batteries [2, 3], functional magnetic and optical materials [4, 5], and electrocatalytic biosensors [6]. From a theoretical perspective, manganese oxides attract great interest due to their strong electron correlations that give rise to complex physical phenomena, including colossal magnetoresistance, charge and orbital ordering, and noncollinear magnetism. Although manganese oxides have been studied extensively, modeling their ground-state magnetic and electronic properties for different oxidation states within density functional theory (DFT) poses fundamental challenges, due to the inherent limitations in the approximations of the exchange-correlation functional. Improvements to these simulations without resorting to higher-level methods and incurring significant computational costs are therefore desirable for large-scale studies of systems involving strongly correlated materials. Here, we construct a pseudopotential that accounts for nonlinear core-valence interactions, and we apply the fully anisotropic DFT+ $U+J$  method. This approach accurately describes the magnetic and electronic properties of bulk manganese oxides with a variety of atomic and magnetic structures and different oxidation states, namely MnO, Mn<sub>3</sub>O<sub>4</sub>,  $\alpha$ -Mn<sub>2</sub>O<sub>3</sub>, and  $\beta$ -MnO<sub>2</sub>.

MnO exists in a  $B1$  rock salt structure with Mn<sup>2+</sup> oxidation state [Fig. 1(a)]. It undergoes paramagnetic to type-II antiferromagnetic (AFM-II) transition at  $T_N = 116$  K, accompanied by cubic ( $Fm\bar{3}m$ ) to rhombohedral structural transition [7]. The ground-state magnetic structure AFM-II consists of ferromagnetically aligned planes that are successively antiparallel along [111] direction. Consequent magnetostriction causes rhombohedral contraction along the [111] below  $T_N$ , tilting the crystal axes  $0.62^\circ$  from the cubic directions [8, 9]. MnO is a charge-transfer insulator with a large band gap of 3.6-4.2 eV measured experimentally [10, 11]. The electronic structure has been studied extensively via first-principles methods, including Hartree-Fock [12–17], LDA [14, 18–20], GGA+ $U$  [15–18, 20–23],  $GW$  method [24], and hybrid functionals [15–17, 21, 25].

Mn<sub>3</sub>O<sub>4</sub> exists in a spinel structure ( $AB_2O_4$ ), with Mn<sup>2+</sup> (Mn<sub>A</sub>) occupying the tetrahedral sites (numbered Mn1-2) and Mn<sup>3+</sup> (Mn<sub>B</sub>) occupying the octahedral sites (numbered Mn3-6) [Fig. 1(b)]. Edge-sharing Mn<sub>B</sub>O<sub>6</sub> octahedra form chains along **a** and **b**. It undergoes cubic ( $Fd\bar{3}m$ ) to tetragonal ( $I4_1/amd$ ) structural transition at 1443 K [26] due to the

56 Jahn-Teller effect at  $\text{Mn}_B$  sites. Strong lattice frustration leads to a rich magnetostructural  
 57 phase diagram at low temperatures. At  $T_N = 42$  K, the material undergoes paramagnetic to  
 58 ferrimagnetic transition [27], adopting a triangular Yafet-Kittel [28] ferrimagnetic (YK-FiM)  
 59 state [29–31]. In the YK-FiM structure,  $\text{Mn}_A$  spins are ferromagnetically aligned along  $\mathbf{b}$ ,  
 60 and  $\text{Mn}_B$  spins are along  $-\mathbf{b}$  canted toward  $\pm\mathbf{c}$  direction [32, 33]. Only a few optical mea-  
 61 surements have been performed, reporting band gaps of 1.91 eV for bulk polycrystalline [34],  
 62 2.51 eV for thin film [35], and 2.07 eV for nanoparticles [36]. The electronic structure of the  
 63 bulk  $\text{Mn}_3\text{O}_4$  spinel has not been studied as extensively as MnO. Computational methods  
 64 including Hartree-Fock [37], GGA+ $U$  and hybrid functionals [21, 34] have been employed  
 65 to simulate the electronic structure using only idealized collinear magnetic structures.

66  $\alpha\text{-Mn}_2\text{O}_3$  has multiple technological applications, such as synthesis substrate for mangan-  
 67 ite oxide perovskite compounds, starting material for lithium ion battery cathode material  
 68  $\text{LiMnO}_2$  [38], and also an environmentally friendly catalyst for water purification [39] and  
 69 combustion [40]. The material exists in a bixbyite structure with  $\text{Mn}^{3+}$  oxidation state [Fig.  
 70 1(c)]. For O chains along  $\mathbf{a}$  or  $\mathbf{b}$ , there is one O atom missing per four sites, such that  
 71 each O atom forms a tetrahedral linkage to surrounding Mn atoms. It undergoes cubic  
 72 ( $Ia3$ ) to orthorhombic ( $Pcab$ ) structural transition at  $T = 308$  K [41] due to the Jahn-Teller  
 73 effect at  $\text{Mn}^{3+}$  sites, causing 0.8% distortion from the cubic structure. The paramagnetic to  
 74 noncollinear-antiferromagnetic (NC-AFM) transition occurs at  $T_{N1} = 80\text{-}90$  K and another  
 75 AFM transition at  $T_{N2} = 25$  K [42–46]. NC magnetic configuration was first proposed  
 76 assuming the cubic structure [45] but was later found to be incompatible with neutron  
 77 powder diffraction data [47]. An alternative collinear AFM structure with four magnetic  
 78 sublattices was proposed by Regulski *et al.* [47] using the cubic lattice (indicated as AFM1  
 79 in this study). However, Cockayne *et al.* [48] found that magnetic sublattice III of the  
 80 AFM1 structure is incompatible with the  $Pcab$  space group, and thereby proposed another  
 81 collinear AFM structure using the orthorhombic lattice (indicated as AFM2 in this study),  
 82 determined independently from both neutron powder diffraction and DFT+ $U$  study. Spin  
 83 canting of  $12\text{-}34^\circ$  was found to further improve the fitting of their diffraction data. Only  
 84 one study reported the optical band gap of 1.2 eV for nanostructures [49]. The electronic  
 85 structure of the bulk material has not been investigated extensively, other than two GGA+ $U$   
 86 studies [21, 48] reporting different results for the magnetic ground state.

87  $\beta\text{-MnO}_2$  is widely used in Li-ion batteries [3, 50–60], Li-O<sub>2</sub> batteries [61, 62], super-

88 capacitors [63–68], adsorbents [69], and catalysts [70, 71].  $\beta$ -MnO<sub>2</sub> exists in a tetragonal  
 89 ( $P4_2/mnm$ ) rutile structure with Mn<sup>4+</sup> oxidation state [Fig. 1(d)]. It undergoes param-  
 90 agnetic to screw-type spiral magnetic transition at  $T_N = 92$  K [72], where the spins lie on  
 91 the  $ab$ -plane and rotate by 129° in the next adjacent layer along the  $c$ -axis for a period  
 92 of 7 unit cells. Transport measurements suggested a very small band gap at low tempera-  
 93 tures [72], with one study reporting a value of 0.26 eV for epitaxially grown thin films [73].  
 94 Computational studies of the bulk material based on idealized MnF<sub>2</sub>-type collinear AFM  
 95 structure were performed using Hartree-Fock [74], GGA+ $U$  [21, 75, 76], and hybrid func-  
 96 tionals [21, 76]. The spiral noncollinear magnetic structure [77] has only been simulated  
 97 using a tight-binding method [78] and dynamical mean-field theory [73].

98 These manganese oxides exhibit complex magnetic and electronic properties, making  
 99 them a challenging set to study. Extensive reports on these systems have shown that rig-  
 100 orous theoretical methods are required to describe their properties adequately [21]. Due  
 101 to the exchange-correlation functional limitations, advanced methods are needed to cor-  
 102 rectly describe the electronic structure of these strongly correlated magnetic materials. The  
 103 strong electronic correlation experienced by the localized  $d$  electrons leads to unphysical  
 104 self-interaction of an electron with the potential it generates. Self-interaction artificially  
 105 raises the energy of the on-site single-particle energies in the Kohn-Sham equations, thereby  
 106 delocalizing the localized electronic states and leading to inaccuracies in the electronic band  
 107 structure. The theoretical methods developed to overcome these inherent limitations in-  
 108 clude DFT+ $U_{\text{eff}}$  [79], DFT+ $U+J$  [80–82], and hybrid functionals [83]. In DFT+ $U_{\text{eff}}$ , where  
 109  $U_{\text{eff}} = U - J$ , an isotropic screened on-site Coulomb interaction is added:

$$E_{\text{Hub}} = \sum_{I,\sigma} \frac{U_{\text{eff}}^I}{2} \text{Tr}[\mathbf{n}^{I\sigma}(\mathbf{1} - \mathbf{n}^{I\sigma})]. \quad (1)$$

110 Here,  $E_{\text{Hub}}$  is the Hubbard correction to the standard approximate DFT energy functional,  
 111  $I$  is the atomic site index,  $\sigma$  is the spin index, and  $\mathbf{n}$  is the occupation matrix. In con-  
 112 trast, Hubbard  $U$  and  $J$  are defined distinctly in DFT+ $U+J$ , leading to a fully anisotropic  
 113 treatment of the Coulomb and exchange matrices accounting for the full orbital dependence:

$$E_{\text{Hub}} = \sum_{I,\sigma} \frac{U^I - J^I}{2} \text{Tr}[\mathbf{n}^{I\sigma}(\mathbf{1} - \mathbf{n}^{I\sigma})] \\ + \sum_{I,\sigma} \frac{J^I}{2} (\text{Tr}[\mathbf{n}^{I\sigma} \mathbf{n}^{I-\sigma}] - 2\delta_{\sigma\sigma_{\text{min}}} \text{Tr}[\mathbf{n}^{I\sigma}]), \quad (2)$$

114 where  $\sigma_{\min}$  denotes the minority spin. Compared with Eq. (1), the extra positive  $J$  term  
115 in Eq. (2) discourages interactions between electrons of antialigned spins on the same site,  
116 thereby encouraging magnetic ordering [82]. This fully anisotropic method has proven to  
117 describe strongly correlated magnetic systems more accurately [76, 84]. The appropriate  $U$   
118 value can enhance or even open up a band gap, and  $J$  can determine the noncollinear mag-  
119 netic ground state, thus refining the electronic structure profile of the system. Additionally,  
120 hybrid functionals have been shown to overcome the deficiencies in describing these mate-  
121 rials (at higher computational cost) by incorporating a fraction of the exact Hartree-Fock  
122 exchange into the exchange-correlation functional. Despite the improvements in results ob-  
123 tained from hybrid functionals, the DFT+ $U$ + $J$  approach is nonetheless a computationally  
124 much cheaper alternative that is desirable in electronic structure studies involving large-scale  
125 systems, such as surfaces, supercells, interfaces, and defects.

126 In this work, we investigate the noncollinear magnetic ground states and the correspond-  
127 ing electronic structures of MnO, Mn<sub>3</sub>O<sub>4</sub>,  $\alpha$ -Mn<sub>2</sub>O<sub>3</sub>, and  $\beta$ -MnO<sub>2</sub> using the DFT+ $U$ + $J$   
128 method. We show that the ground-state lattice, magnetism, and electronic structure pro-  
129 file can be obtained with accuracy nearing that of literature hybrid functional calculations,  
130 through careful pseudopotential design and selection of fully anisotropic  $U$  and  $J$  values.

## 131 II. METHOD AND COMPUTATIONAL DETAILS

132 The magnetic and electronic structures of the manganese oxides are calculated with first-  
133 principles DFT using the PBEsol [85] parametrization of the generalized gradient approx-  
134 imation with on-site Coloumb repulsion and exchange parameters  $U$  and  $J$ , treated sep-  
135 arately and explicitly defined within the rotationally invariant, fully anisotropic scheme  
136 (DFT+ $U$ + $J$ ) [81, 82], using the atomic orbital projection scheme [86] as implemented in  
137 the QUANTUM ESPRESSO [87] package. It has been demonstrated that the fully anisotropic  
138  $J$  parameter plays an important role in describing strongly correlated noncollinear antiferro-  
139 magnetic systems [76]. We determine the optimal Hubbard  $U$  and  $J$  values by first testing  
140 a range of values reported in the literature and changing the values as necessary, each time  
141 observing the effect on the ground-state magnetic and electronic structures and properties.  
142 We also employed the linear response method by Cococcioni *et al.* [88] to determine a range  
143 of  $U$  values; however, the values obtained by this method were too high ( $> 7$  eV) for ac-

144 curate electronic structure profiles. The calculations account for spin-polarized electronic  
 145 densities by treating the Mn magnetic moments as noncollinear for all systems. All atoms  
 146 are represented by norm-conserving, optimized [89], designed nonlocal [90] pseudopotentials  
 147 generated with the OPIUM package [91], treating the  $2s$  and  $2p$  of O and  $3s$ ,  $3p$ ,  $3d$ ,  $4s$ , and  
 148  $4p$  of Mn as valence states. In addition to the treatment of semicore states as valence by  
 149 this Mn pseudopotential, nonlinear core-valence interaction via the partial core correction  
 150 scheme [92–94] is incorporated to account for the non-negligible overlap between the core  
 151 and the valence states. All calculations are run with a 70 Ry plane-wave energy cutoff to  
 152 ensure accuracy for small relative energies among different magnetic configurations. The  
 153 Brillouin zone is sampled using Monkhorst-Pack [95]  $k$ -point meshes of dimensions  $6 \times 6 \times 6$ ,  
 154  $8 \times 8 \times 8$ ,  $4 \times 4 \times 4$ , and  $6 \times 6 \times 6$  for MnO, Mn<sub>3</sub>O<sub>4</sub>,  $\alpha$ -Mn<sub>2</sub>O<sub>3</sub>, and  $\beta$ -MnO<sub>2</sub>, respectively.  
 155 A  $12 \times 12 \times 12$   $k$ -point grid is used for post-processing the electronic structure calculations  
 156 for all four systems. All relaxations starting from the experimental crystal structures are  
 157 performed without  $U$  and  $J$ , as relaxation with  $U$  leads to overestimated lattices and bond  
 158 lengths [21]. The magnetic and electronic structures of the optimized crystal structures are  
 159 then refined with  $U$  and  $J$ .

### 160 III. RESULTS AND DISCUSSION

161 Throughout this section, our results on the ground-state structural, magnetic, and elec-  
 162 tronic properties of the four manganese oxide systems are discussed in detail with respect to  
 163 the computational parameters employed and in comparison with previously published data.  
 164 Table I provides an overview of the results for each manganese oxide system from both exper-  
 165 imental and computational studies, including DFT+ $U$ (+ $J$ ) and hybrid functional studies  
 166 from the literature, in comparison to our PBEsol+ $U$ + $J$  study.

#### 167 A. MnO

168 Crystal structure relaxations with various imposed magnetic orders, antiferromagnetic  
 169 (AFM-II, A-AFM, C-AFM) and ferromagnetic (FM), reveal the AFM-II structure as the  
 170 magnetic ground state (Table II). The lattice constant,  $a = 4.40 \text{ \AA}$ , is 0.68 % smaller than the  
 171 literature value of  $4.43 \text{ \AA}$  [96]. PBEsol therefore yields structural properties that are in good

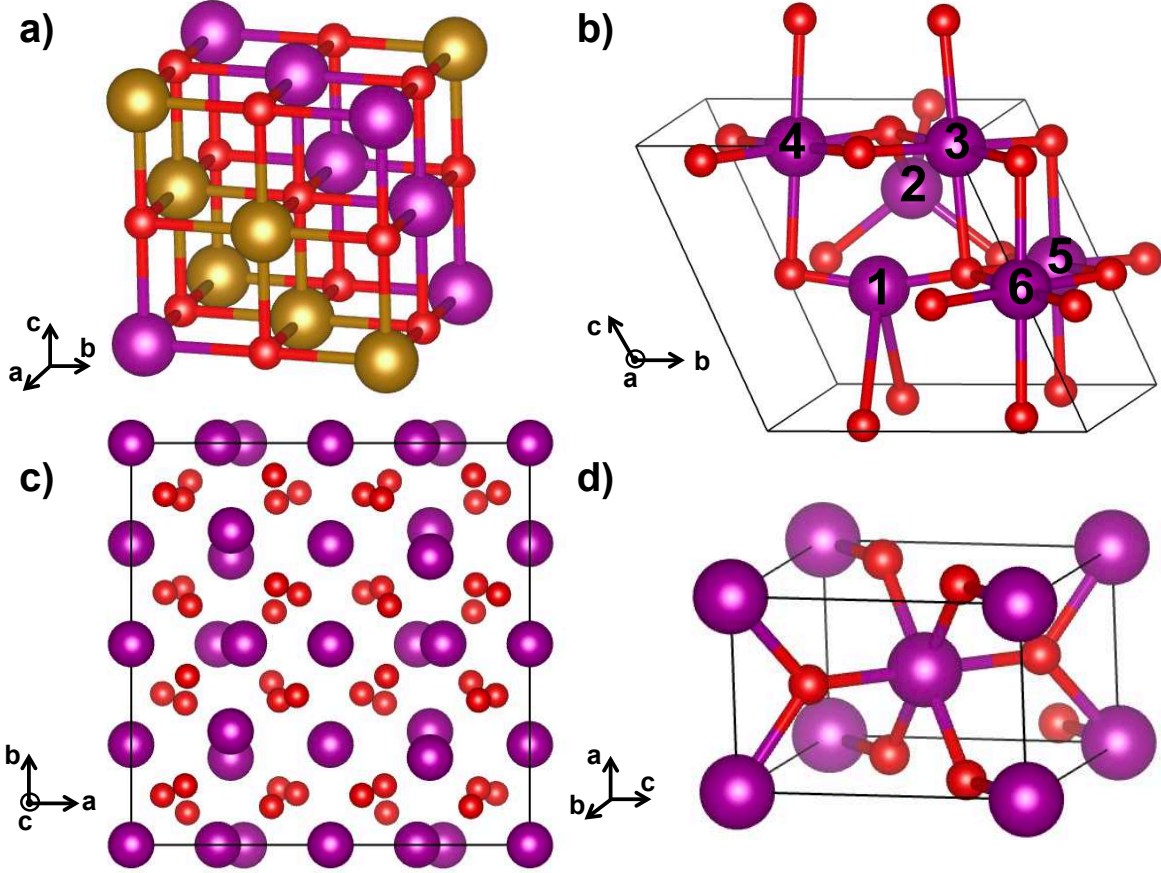


FIG. 1. Optimized crystal structures of the manganese oxides in their magnetic ground states: (a) AFM-II MnO, (b) YK-FiM Mn<sub>3</sub>O<sub>4</sub>, (c) NC-AFM2  $\alpha$ -Mn<sub>2</sub>O<sub>3</sub>, and (d) spiral  $\beta$ -MnO<sub>2</sub>. Spin-up and spin-down Mn are colored in purple and gold for MnO, respectively, with red O atoms. The magnetic ground states of Mn<sub>3</sub>O<sub>4</sub>,  $\alpha$ -Mn<sub>2</sub>O<sub>3</sub>, and  $\beta$ -MnO<sub>2</sub> are noncollinear; these spin structures are further discussed and illustrated in the Results and Discussion section. Bonds are not shown in (c) for clearer observation of the O chains along **a** or **b**.

172 agreement with the experimental values. Other AFM orders result in  $c < a$ , inconsistent  
 173 with experimental data, while FM order produces a severely contracted lattice structure.

174 Electronic structure calculation without  $U$  and  $J$  shows an underestimated band gap  
 175 of 1.16 eV, consistent with previous GGA studies [15–18, 20, 23]. Applying  $U = 4$  eV  
 176 increases the band gap to 3.32 eV; this value is higher compared to other DFT+ $U_{\text{eff}}$ . For  
 177 example, Franchini *et al.* [16] obtained a band gap of 2.03 eV with  $U = 6$  eV; they were  
 178 able to increase the band gap to 3 eV only by increasing the  $U$  value up to 15 eV. Since our  
 179 calculation requires much lower  $U$  value to achieve a more reasonable band gap, it suggests



TABLE I. Ground-state magnetism, lattice, magnetic moment per Mn, and band gap for each manganese oxide system reported by (1) experimental studies, (2) literature DFT+ $U(+J)$ , and (3) literature hybrid functional studies, in direct comparison to (4) our PBEsol+ $U+J$  results. Our lattice constants presented here are values optimized without  $U$  and  $J$ .

System	Method	Magnetic state	Lattice constants (Å)	Mag. mom. ( $\mu_B$ )	$E_g$ (eV)
MnO	(1) Experimental	AFM-II	$a=4.43$ [96]	4.58 [97]	3.6-4.2 [10, 11]
	(2) PBE+ $U$ , $U=4$ eV [23]	AFM-II	$a=4.489$	4.60	2.34
	(3) PBE0 [16]	AFM-II	$a=4.40$	4.52	4.02
	(4) PBEsol+ $U+J$ , $U=4$ eV, $J=1.2$ eV	AFM-II	$a=4.40$	4.56	2.81
Mn <sub>3</sub> O <sub>4</sub>	(1) Experimental	YK-FiM	$a=5.71$ , $c=9.35$ [33] $V_0=155.73\text{Å}^3$ [98]	4.34, 3.64, 3.25 [33]	1.91 [34]
	(2) PBE+ $U$ , $U=5$ eV [34]	FiM6	N/A	4.6, 3.9	1.46
	(3) PBE0 [21]	FiM3	$V_0=157.42\text{Å}^3$	3.69-4.50	2.4
	(4) PBEsol+ $U+J$ , $U=4$ eV, $J=1.2$ eV	YK-FiM	$a=5.76$ , $c=9.35$ $V_0=155.50\text{Å}^3$	4.49, 3.74, 3.69	1.01
$\alpha$ -Mn <sub>2</sub> O <sub>3</sub>	(1) Experimental	NC-AFM2 [48]	$a=9.407$ , $b=9.447$ , $c=9.366$ , $V_0=834.48\text{Å}^3$ [41]	3.3-4.0 [47] 2.6-3.5 [48]	1.2 [49]
	(2) PBEsol+ $U+J$ , $U=2.8$ eV, $J=1.2$ eV [48]	AFM2	$a=9.402$ , $b=9.444$ , $c=9.367$	3.6	0.6
	(3) HSE [21]	FM	$V_0=845.83\text{Å}^3$	3.81-3.84	0.1
	(4) PBEsol+ $U+J$ , $U=2.8$ eV, $J=1.2$ eV	NC-AFM2	$a=9.382$ , $b=9.444$ , $c=9.376$ , $V_0=830.71\text{Å}^3$	4.09, 2.91, 3.68, 3.83, 3.69	0.081
$\beta$ -MnO <sub>2</sub>	(1) Experimental	Spiral	$a=4.396$ , $c=2.871$ $V_0=55.48\text{Å}^3$ [99]	2.35 [100]	0.26 [73]
	(2) GGA+ $U+J$ , $U=6.7$ eV, $J=1.2$ eV [76]	AFM	$a=4.45$ , $c=2.936$	2.96	0.8
	(3) PBE0 [21]	AFM	$V_0=55.06\text{Å}^3$	2.89	1.5
	(4) PBEsol+ $U+J$ , $U=2.8$ eV, $J=1.2$ eV	Spiral	$a=4.402$ , $c=2.880$ $V_0=55.80\text{Å}^3$	2.63	0.25

180 enhanced performance of our designed pseudopotential.

181 Despite moving the band gap closer to the experimental value, the electronic structure  
182 profile is compromised by  $U$  when compared with those reported by hybrid functional cal-  
183 culations [15–17, 21, 25], as  $U$  shifts the energies of the valence and conduction bands  
184 further apart. Previous  $GW$  studies reported that large values of  $U$  reorder the bands when  
185 compared to the  $GW$  quasiparticle band structures [24, 101]. We find that applying an  
186 anisotropic  $J = 1.2$  eV enhances the profile significantly, but it reduces the band gap to  
187 2.81 eV [Fig. 2(a)]. Explicitly defined Hubbard  $J$  takes into account the full symmetry of  
188  $d$ - $d$  interactions, thereby providing a better description of orbital spin polarizations [76]. In  
189 our orbital-projected density of states (DOS), the highest-energy valence band shows strong  
190 mixing of O  $2p$  and Mn  $e_g$  states enhanced by  $U$ , whereas the lowest-energy conduction band  
191 primarily consists of Mn  $t_{2g}$  states. Together with the calculated magnetic moment of 4.56

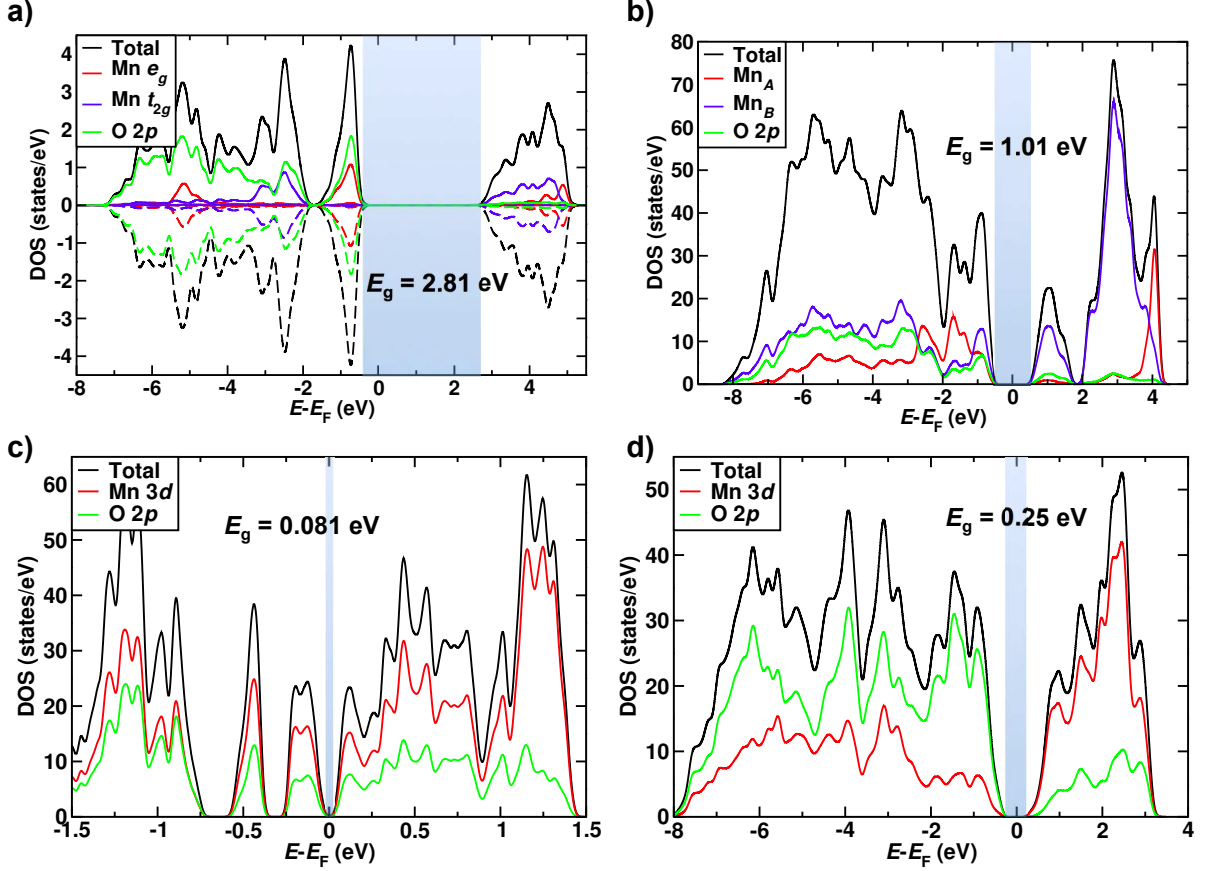


FIG. 2. Projected density of states of the manganese oxides computed with PBEsol+ $U+J$ : (a) MnO shows a collinear AFM-II ground state with a bandgap of 2.81 eV; the valence bands are governed by the overlap between O 2p and Mn  $e_g$  orbitals, and the conduction bands by Mn  $t_{2g}$  orbitals. The rest of the systems have noncollinear magnetic ground states: (b)  $\text{Mn}_3\text{O}_4$  shows a YK-FiM ground state with a band gap of 1.01 eV, where  $\text{Mn}_A$  and  $\text{Mn}_B$  refer to the tetrahedral and the octahedral sites, respectively; (c)  $\alpha\text{-Mn}_2\text{O}_3$  shows a NC-AFM2 ground state with a small band gap of 0.081 eV; (d)  $\beta\text{-MnO}_2$  shows a spiral magnetic ground state with a band gap of 0.25 eV. The band gap regions are indicated with a light blue color.

192  $\mu_B$ , in good agreement with the experimental value of  $4.58 \mu_B$  [97], our electronic structure  
 193 predicts MnO as a high-spin insulator of intermediate Mott-Hubbard/charge-transfer char-  
 194 acter, consistent with results from previous high-level computational studies [12, 15–17, 25].

TABLE II. Relaxed lattice constants and relative energies per formula unit of MnO with various imposed magnetic orders. Experimental lattice constant is  $a = 4.43 \text{ \AA}$  [96] with the AFM-II ground state.

Magnetism	Lattice constants ( $\text{\AA}$ )	Relative $E$ (meV/f.u.)
AFM-II	$a = 4.40$	0
C-AFM	$a = 4.41, c = 4.38$	17
A-AFM	$a = 4.43, c = 4.38$	80
FM	$a = 4.29$	413

## B. $\text{Mn}_3\text{O}_4$

We determine the ground-state magnetic structure of  $\text{Mn}_3\text{O}_4$  to be the experimentally reported YK-FiM structure. This noncollinear structure is 152 meV lower in energy than the lowest collinear structure. The YK-FiM structure has not been computed before; therefore, we start by comparing our results with previous calculations on idealized collinear structures. We compute the six idealized collinear FiM configurations (FiM1-6), in addition to the FM order, as first specified in the Hartree-Fock study of Chartier *et al.* [37]. Six Mn atoms of the unit cell are numbered as shown in Fig. 1(b), where two  $\text{Mn}_A$  are Mn1-2, two  $\text{Mn}_B$  along  $\mathbf{b}$  are Mn3-4, and two  $\text{Mn}_B$  along  $\mathbf{a}$  are Mn5-6. Crystal structure relaxation with the six imposed FiM orders shows FiM6 ( $\uparrow\downarrow\uparrow\downarrow\uparrow\downarrow$ ) as the lowest-energy structure when the spins are held collinear. In FiM6 order, all spins are antiferromagnetic to all their neighbors, which is consistent with the experimental measurements reporting the exchange interaction constants to be antiferromagnetic [31, 102, 103]. However, the net magnetic moment is zero in FiM6, which is inconsistent with the experimentally observed net magnetic moment of  $1.84 \mu_B$  per formula unit along  $\mathbf{b}$  [30, 32, 33, 104]. The idealized collinear FiM configuration most consistent with the experimentally observed YK-FiM structure would be FiM4 ( $\uparrow\uparrow\downarrow\uparrow\downarrow$ ), where  $\text{Mn}_A$  spins (Mn1-2) are ferromagnetically aligned, and all  $\text{Mn}_B$  spins (Mn3-6) are antiferromagnetically aligned. We find that applying  $U = 4 \text{ eV}$  and  $J = 1.2 \text{ eV}$  to the relaxed structures lowers the energy of the FiM4 structure, making it the lowest-energy collinear magnetic state (Table III). However, once the spins are allowed to be noncollinear, the YK-FiM structure is the most energetically favorable. The lattice constants obtained

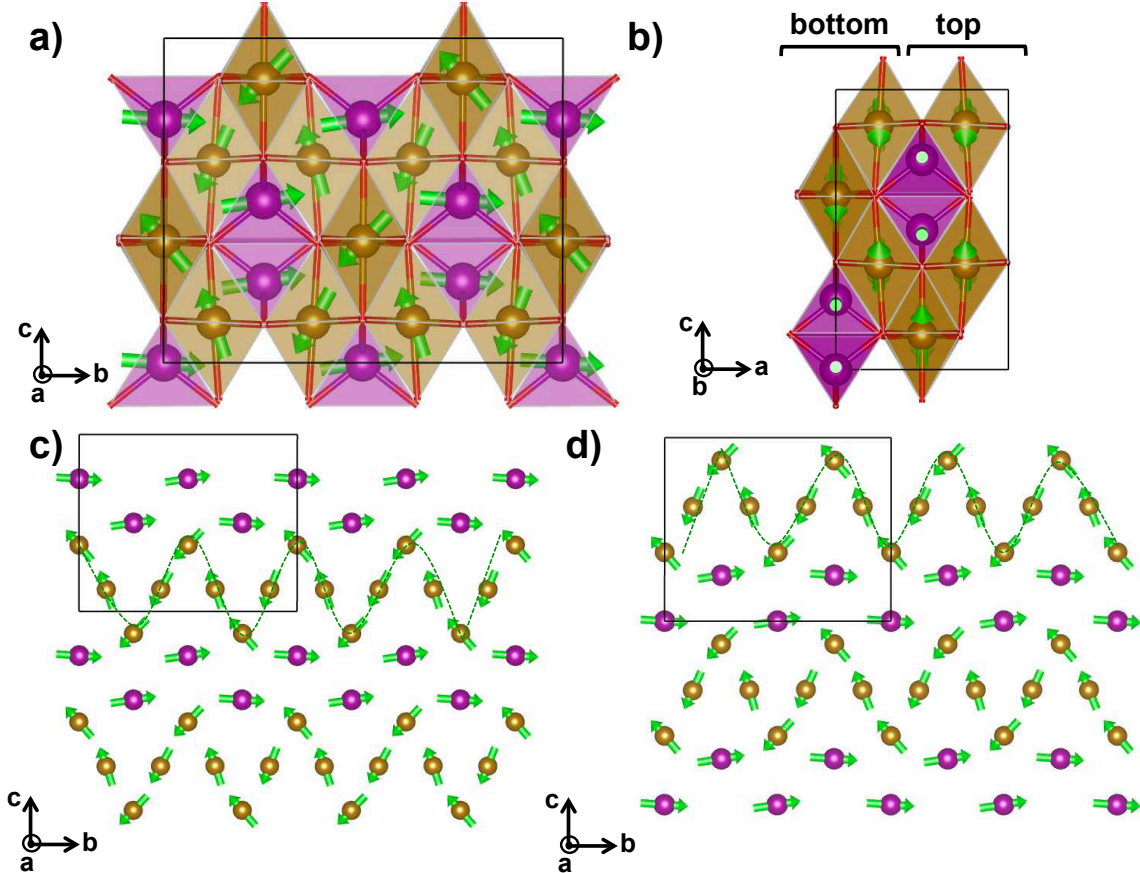


FIG. 3. Computed YK-FiM structure of  $\text{Mn}_3\text{O}_4$ : (a) Magnetic moments are colored in green within the Mn tetrahedral (purple) and octahedral (gold) cages; (b) Side view showing the top and bottom bilayers used to illustrate the noncollinear spin pattern; (c) Top bilayer exhibiting a sinusoidal  $\text{Mn}_B$  spin pattern (along the green dashed lines), with  $\text{Mn}_A$  spin alignment along the  $b$ -axis; (d) the bottom bilayer shows a similar spin structure, but the pattern is related by mirror symmetry to the one shown in (c).

216 with FiM4 order are  $a = 5.76 \text{ \AA}$  and  $c = 9.35 \text{ \AA}$ , in good agreement with the experimental  
 217 values of  $a = 5.71 \text{ \AA}$  and  $c = 9.35 \text{ \AA}$  reported by neutron diffraction study of a single-crystal  
 218 sample [33].

219 In contrast to our results, previous computational studies reported FiM3 ( $\uparrow\uparrow\downarrow\downarrow\uparrow\uparrow$ ) [21]  
 220 and FiM6 ( $\uparrow\downarrow\uparrow\downarrow\uparrow\downarrow$ ) [34, 37] as the magnetic ground state. FiM3 order describes intrachain  
 221  $B$ - $B$  interactions to be ferromagnetic, which is inconsistent with the experimental obser-  
 222 vations of the interaction to be strongly antiferromagnetic [31, 102, 103, 105]. To justify  
 223 FiM4 ( $\uparrow\uparrow\uparrow\downarrow\uparrow\downarrow$ ) as the idealized collinear magnetic ground state, we calculated four exchange

TABLE III. Relaxed lattice constants of  $\text{Mn}_3\text{O}_4$  with various imposed magnetic orders, in addition to relative energies per formula unit and magnetic moments per Mn obtained with  $U = 4$  eV and  $J = 1.2$  eV. Experimental lattice constants are  $a = 5.71$  Å and  $c = 9.35$  Å, and the experimental magnetic moments are 4.34, 3.64, and 3.25  $\mu_B$  for tetrahedral Mn, octahedral Mn along  $b$ , and octahedral Mn along  $a$ , respectively [33] with the YK-FiM ground state.

Magnetism	Lattice constants (Å)	Relative $E$ (meV/f.u.)	Magnetic moment ( $\mu_B$ )
YK-FiM	$a = 5.76, c = 9.35$	0	4.49, 3.74, 3.69
FiM4 ( $\uparrow\uparrow\uparrow\downarrow\downarrow$ )	$a = 5.76, c = 9.35$	152	4.50, 3.85, 3.65
FiM1 ( $\downarrow\downarrow\uparrow\uparrow\uparrow$ )	$a = 5.74, c = 9.37$	154	4.48, 3.67
FiM6 ( $\uparrow\downarrow\uparrow\downarrow\downarrow$ )	$a = 5.76, b = 5.78, c = 9.32$	158	4.48, 3.76
FiM3 ( $\uparrow\uparrow\downarrow\uparrow\uparrow$ )	$a = 5.75, c = 9.34$	175	4.50, 3.85, 3.65
FiM2 ( $\uparrow\downarrow\uparrow\uparrow\uparrow$ )	$a = 5.77, c = 9.35$	184	4.51, 3.78
FiM5 ( $\uparrow\uparrow\uparrow\downarrow\uparrow$ )	$a = 5.81, b = 5.78, c = 9.36$	193	4.50, 3.86, 3.66
FM ( $\uparrow\uparrow\uparrow\uparrow\uparrow$ )	$a = 5.82, c = 9.36$	208	4.52, 3.87

224 interaction constants:  $J_{AA}$ ,  $J_{AB}$ ,  $J_{BBsr}$ , and  $J_{BBlr}$ , where the last two values represent in-  
225 trachain (short-range) and interchain (long-range)  $B$ - $B$  interactions, respectively. We map  
226 the energies of the six FiM structures, relative to that of the FM structure, to a Heisenberg  
227 Hamiltonian, as described in Ref. [37]. All interactions are antiferromagnetic, with small  
228 values involving the tetrahedral  $\text{Mn}_A$  site ( $J_{AA} = -0.36$  K and  $J_{AB} = -2.98$  K), large and dom-  
229 inant intrachain  $B$ - $B$  interaction ( $J_{BBsr} = -23.9$  K), and small interchain  $B$ - $B$  interaction  
230 ( $J_{BBlr} = -0.45$  K). The  $J$  values are in reasonable agreement with the experimental values  
231 obtained from a polycrystalline sample [31] ( $J_{AA} = -4.9$  K,  $J_{AB} = -6.8$  K, and  $J_{BB} = -19.9$   
232 K). The strong antiferromagnetic intrachain  $B$ - $B$  interaction can be understood as a result  
233 of the direct exchange between overlapping neighboring  $\text{Mn}_B$   $t_{2g}$  orbitals ( $J_{BBsr}$ ) dominating  
234 over very weak ferromagnetic superexchange mediated by O  $2p$  orbitals ( $J_{BBlr}$ ) [103].

235 The noncollinear magnetic ground state shows an exotic spin pattern, illustrated in Fig.  
236 3. All the spins lie on the  $bc$  plane.  $\text{Mn}_A$  spins are aligned along the  $b$ -axis, as if they were  
237 ferromagnetic in that direction, with small deviations from the  $b$ -axis. However,  $\text{Mn}_B$  spins  
238 show a sinusoidal spin pattern that is related by mirror symmetry for different bilayers of  
239 the system [Fig. 3(c) and (d)]. Calculating the electronic structure of the YK-FiM ground

240 state with  $U = 4$  eV and  $J = 1.2$  eV yields a band gap of 1.01 eV [Fig. 2(b)]. This opening  
 241 of a gap is remarkable when compared with the PBE+ $U$  study of Franchini *et al.* [21],  
 242 where only half-metallic states with gaps of 0.3-0.5 eV were obtained with  $U = 3-6$  eV for  
 243 FiM3 order. Since our noncollinear magnetic ground state is the experimentally reported  
 244 structure, YK-FiM, rather than FiM3 [21] or FiM6 [34, 37], the electronic structure profile  
 245 cannot be directly compared with those reported by the previous computational studies.  
 246 However, several features are in agreement. The valence band consists of widely spread Mn  
 247  $3d$  states with a large mixing of O  $2p$  states. The conduction band mostly consists of Mn<sub>B</sub>  
 248  $3d$  states, with a characteristic splitting of  $\approx 0.21$  eV, which was also reported by Hirai *et*  
 249 *al.* [34] as well. The calculated magnetic moments are 4.49, 3.74, and 3.69  $\mu_B$  for the spins of  
 250 Mn<sub>A</sub>, Mn<sub>B</sub> along  $b$ , and Mn<sub>B</sub> along  $a$ , respectively, in good agreement with the experimental  
 251 values of 4.34, 3.64, and 3.25  $\mu_B$  reported by neutron diffraction study of a single-crystal  
 252 sample [33]. The splitting of Mn<sub>B</sub> magnetic moment was also observed by a  $^{55}\text{Mn}$  NMR  
 253 study [106]. Our study predicts Mn<sub>3</sub>O<sub>4</sub> as an insulator with the YK-FiM ground state, in  
 254 agreement with the experimental reports.

### 255 C. $\alpha\text{-Mn}_2\text{O}_3$

256 We compute the magnetic and electronic structures of  $\alpha\text{-Mn}_2\text{O}_3$  using the AFM or-  
 257 derings proposed by Regulski *et al.* [47] (AFM1) and Cockayne *et al.* [48] (AFM2) while  
 258 allowing spin noncollinearity. Cockayne *et al.* [48] determined the NC-AFM2 order to be  
 259 the magnetic ground state [Fig. 4(a)-(b)], independently from neutron powder diffraction  
 260 and PBEsol+ $U+J$  study in concurrence with a cluster-expansion model, suggesting that  
 261 the ground-state magnetic structure of  $\alpha\text{-Mn}_2\text{O}_3$  has largely been solved. In agreement with  
 262 this observation, our structural, electronic, and magnetic relaxations with each candidate  
 263 magnetic order confirm the NC-AFM2 structure as the magnetic ground state [Fig. 4(a)].  
 264 Applying  $U = 2.8$  eV and  $J = 1.2$  eV further stabilizes the NC-AFM2 structure (Table  
 265 IV). This complex spin structure is easier to understand in terms of four magnetic sublattices  
 266 [Fig. 4(c) and (d)]. These four magnetic sublattices correspond to the Mn Wyckoff  
 267 positions: sublattice I consists of Mn 4(a) and Mn 4(b), and sublattices II-IV consist of Mn  
 268 8(c) with different spin patterns. The spin deviation from the  $c$ -axis varies from 4-23°, as  
 269 shown in Table V, in general agreement with the experimental work, where the spins deviate

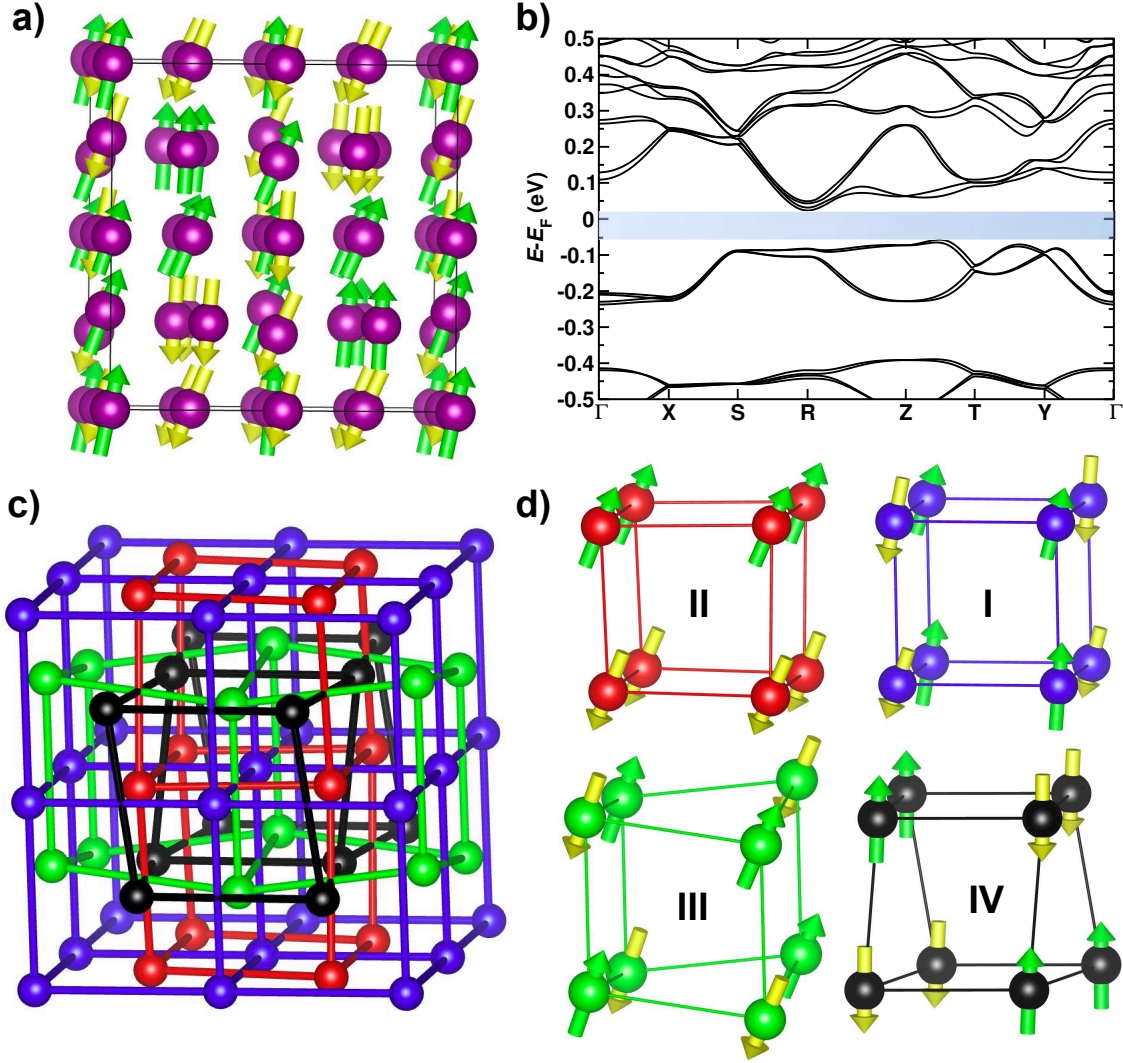


FIG. 4. Magnetic and electronic structures of  $\alpha$ - $\text{Mn}_2\text{O}_3$ : (a) Computed NC-AFM2 structure, with green and yellow spins indicating up and down directions, respectively; (b) The corresponding band structure shows an insulating state with a gap of 0.081 eV; (c) Four magnetic sublattices based on Mn Wyckoff positions; (d) The magnetic sublattices from (c) untangled for clarity, where sublattice I consists of Mn 4(a) and 4(b) in a C-type magnetic structure, sublattice II consists of Mn 8(c) in an A-type magnetic structure, sublattice III consists of Mn 8(c) in a G-type magnetic structure, and sublattice IV consists of Mn 8(c) in a unique magnetic structure, where each magnetic ion has three nearest neighbors, one with identical spin direction and two with opposite spin direction, similar to E-type [107].

270 in a range of  $12$ - $34^\circ$ . More importantly, our computed electronic structure shows a band  
 271 gap of 0.081 eV [Fig. 4(b)]. Although our results are consistent with the experimental and

272 theoretical work presented by Cockayne *et al.* [48], they are in disagreement with the results  
 273 reported by Franchini *et al.* [21], where both PBE+ $U$  and hybrid functional calculations,  
 274 HSE and PBE0, yielded FM ground state. This disagreement suggests that those levels  
 275 of theory incorrectly predict the ground state of this complex magnetic system and that a  
 276 noncollinear description of this system is needed. As for the lattice structure, relaxation  
 277 with the AFM2 order yields  $a = 9.382 \text{ \AA}$ ,  $b = 9.444 \text{ \AA}$ , and  $c = 9.376 \text{ \AA}$ , in good agreement  
 278 with the experimental values of  $a = 9.408 \text{ \AA}$ ,  $b = 9.449 \text{ \AA}$ , and  $c = 9.374 \text{ \AA}$  [48].

279 TABLE IV. Relaxed lattice constants of  $\alpha$ -Mn<sub>2</sub>O<sub>3</sub> with various imposed magnetic orders, in addi-  
 280 tion to relative energies per formula unit obtained with  $U = 2.8 \text{ eV}$  and  $J = 1.2 \text{ eV}$ . Experimental  
 281 lattice constants are  $a = 9.407 \text{ \AA}$ ,  $b = 9.447 \text{ \AA}$ , and  $c = 9.366 \text{ \AA}$  [41] with the NC-AFM2 ground  
 282 state [48].

Magnetism	Lattice constants ( $\text{\AA}$ )	Relative $E$ (meV/f.u.)
NC-AFM2	$a = 9.382, b = 9.444, c = 9.376$	0
NC-AFM1	$a = 9.410, b = 9.387, c = 9.399$	4.1
FM	$a = 9.438$	50

285 TABLE V. Magnetic moments per Mn and spin angles for the NC-AFM2 structure of  $\alpha$ -Mn<sub>2</sub>O<sub>3</sub>,  
 286 based on the five unique Mn Wyckoff positions. The spin angles are relative to the  $c$ -axis. The  
 287 experimental magnetic moments are in the range of  $2.6\text{-}4.0 \mu_B$  [47, 48].

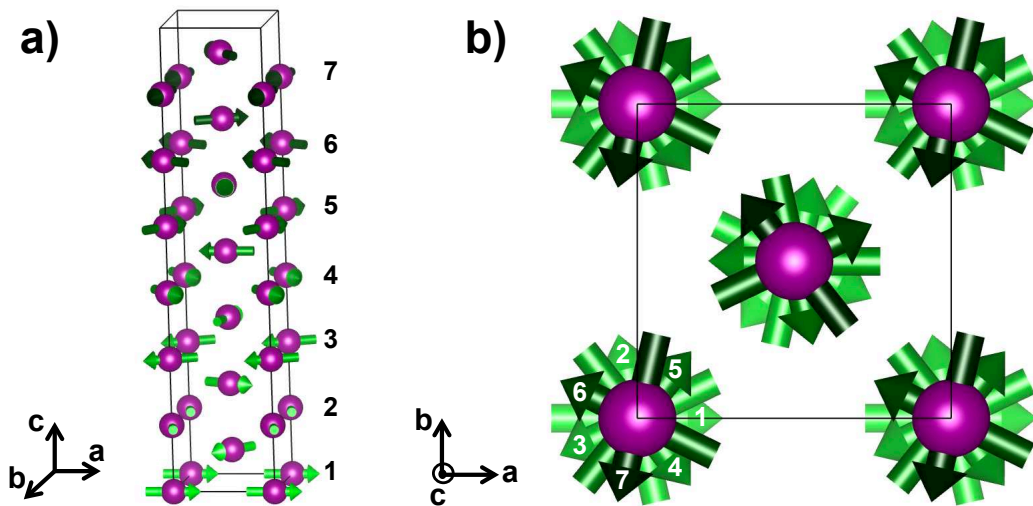
Mn Wyckoff position	Magnetic moment ( $\mu_B$ )	Spin angle ( $^\circ$ )
Mn 4(a)	4.09	8.7
Mn 4(b)	2.91	17.3
Mn 8(c)	3.68	23.4
Mn 8(c)	3.83	21.8
Mn 8(c)	3.69	4.5

290 Calculating the electronic structure of the NC-AFM2 order with  $U = 2.8 \text{ eV}$  and  $J = 1.2$   
 291  $\text{eV}$  yields an insulating state with a gap of  $0.081 \text{ eV}$  [Fig. 2(c)], with the projected DOS pro-  
 292 file in good agreement with that reported by Cockayne *et al.* [48]. The calculated magnetic  
 293 moments, shown in Table V, are in general agreement with the experimental values of Cock-



294 ayne *et al.* [48], which vary from 2.6-4.0  $\mu_B$ . Within the framework of DFT+ $U$ + $J$ , our study  
 295 predicts  $\alpha$ -Mn<sub>2</sub>O<sub>3</sub> as an insulator with the NC-AFM2 ground state, in agreement with the  
 296 experimental observations. Achieving accurate magnetic properties with our computational  
 297 setup is a significant leap forward to understanding these complex magnetic systems.

298 **D.  $\beta$ -MnO<sub>2</sub>**



300 FIG. 5. Computed spiral magnetic structure of  $\beta$ -MnO<sub>2</sub>: (a) Side view showing the seven unit cell  
 301 period of the spin spiral, numbered for clarity, with magnetic moments colored in green; (b) Top  
 302 view showing the spin rotation of 129° from each layer. The darker the spin, the closer it is to the  
 303 viewer.

304 To compute the magnetic structure of  $\beta$ -MnO<sub>2</sub>, we use the screw-type spiral order, in  
 305 addition to the AFM and FM orders that previous computational studies have employed [21,  
 306 74–76]. Crystal and magnetic structure relaxations yield the spiral structure as the magnetic  
 307 ground state (Table VI). The lattice constants,  $a = 4.402$  Å and  $c = 2.880$  Å, are in excellent  
 308 agreement with the experimental values of  $a = 4.404$  Å and  $c = 2.877$  Å [108, 109]. The  
 309 spiral structure [Fig. 5] consists of spins on the  $ab$ -plane rotating by 129° across each layer  
 310 along the  $c$ -axis. A total of seven unit cells (14 layers) are needed for a complete magnetic  
 311 spiral period (5 spin revolutions).

312 Calculating the electronic structure of the spiral order with  $U = 2.8$  eV and  $J = 1.2$   
 313 eV yields an insulating state with a gap of 0.25 eV [Fig. 2(d)], in good agreement with the

TABLE VI. Relaxed lattice constants of  $\beta$ -MnO<sub>2</sub> with different imposed magnetic orders, in addition to relative energies per formula unit and magnetic moments per Mn obtained with  $U = 2.8$  eV and  $J = 1.2$  eV. Experimental lattice constants are  $a = 4.396$  Å and  $c = 2.871$  Å [99], and the magnetic moment is  $2.35 \mu_B$  [100] with the spiral magnetic ground state.

Magnetism	Lattice constants (Å)	Relative $E$ (meV/f.u.)	Magnetic moment ( $\mu_B$ )
Spiral	$a = 4.402, c = 2.88$	0	2.63
AFM	$a = 4.402, c = 2.88$	47	2.65
FM	$a = 4.422, c = 2.89$	650	2.91

314 value of 0.27 eV reported by PBEsol+ $U+J$  study [75] and 0.26 eV reported by optical mea-  
315 surements of a thin film sample [73]. Similar to Mn<sub>3</sub>O<sub>4</sub>, the opening of a gap is remarkable  
316 when compared with PBE+ $U$  study of Franchini *et al.* [21], where only metallic states were  
317 obtained with  $U$  values up to 6 eV. The projected DOS profile is also in excellent agreement  
318 with that reported by hybrid functional calculations of Franchini *et al.* [21]. In accordance  
319 with the Mn<sup>4+</sup> oxidation state and the octahedral crystal-field splitting, the valence band  
320 shows a single broad Mn  $t_{2g}$  band with a large mixing of O  $2p$  states, whereas the conduc-  
321 tion band consists mostly of Mn  $e_g$  states with small O  $2p$  mixing. The calculated magnetic  
322 moment of  $2.63 \mu_B$  is in good agreement with the experimental value of  $2.35 \mu_B$  reported by  
323 neutron powder diffraction study [100]. Our electronic structure accurately predicts  $\beta$ -MnO<sub>2</sub>  
324 as an insulator with the spiral magnetic ground state.

#### 325 IV. SUMMARY AND CONCLUSIONS

326 Our computational study of manganese oxides, using the fully anisotropic PBEsol+ $U+J$   
327 approach, yields ground-state structural, magnetic, and electronic properties of quality and  
328 accuracy that are comparable to previously reported hybrid functional and experimental  
329 studies. We show that the limitations of conventional DFT regarding the magnetic and  
330 electronic structures of insulating transition metal oxides can be improved by pseudopotential  
331 design and careful selection of fully anisotropic  $U$  and  $J$  values. The resulting magnetic  
332 ground states (AFM-II, YK-FiM, NC-AFM2, and spiral for MnO, Mn<sub>3</sub>O<sub>4</sub>,  $\alpha$ -Mn<sub>2</sub>O<sub>3</sub>, and  $\beta$ -  
333 MnO<sub>2</sub>, respectively) correspond to the experimentally observed configurations. All relaxed

334 lattice constants, obtained with PBEsol alone, are in good agreement with the experimental  
335 values. Appropriate band gaps were obtained with  $U$  values smaller than those used by  
336 previous GGA+ $U$  studies, while reproducing the electronic structure profiles in good agree-  
337 ment with those reported by previous hybrid functional studies. Our results overall suggest  
338 the enhanced performance of our designed pseudopotential with semicore and partial core  
339 correction, thereby offering a promising potential of the DFT+ $U+J$  approach for electronic  
340 structure studies involving other strongly correlated, complex magnetic systems with accu-  
341 racy nearing that of more computationally expensive methods such as hybrid functionals.

## 342 ACKNOWLEDGEMENTS

343 The authors acknowledge support from the Department of Energy, Division of Basic  
344 Energy Sciences, under grant DE-FG02-07ER15920. J. S. L. wishes to thank the Vagelos  
345 Integrated Program in Energy Research (VIPER) at the University of Pennsylvania. Com-  
346 putational support was provided by the High-Performance Computing Modernization Office  
347 and the National Energy Research Scientific Computing Center.

- 
- 348 [1] Z. Yang, Y. Zhang, W. Zhang, X. Wang, Y. Qian, X. Wen, and S. Yang, *J. Solid State*  
349 *Chem.* **17**, 679 (2006).
- 350 [2] M. M. Thackeray, W. I. F. David, P. G. Bruce, and J. B. Goodenough, *Mater. Res. Bull.*  
351 **18**, 461 (1983).
- 352 [3] M. M. Thackeray, *Prog. Solid State Chem.* **25**, 1 (1997).
- 353 [4] G. H. Lee, S. H. Huh, J. W. Jeong, B. J. Choi, S. H. Kim, and H.-C. Ri, *J. Am. Chem. Soc.*  
354 **124**, 12094 (2002).
- 355 [5] S. Thota, B. Prasad, and J. Kumar, *Mater. Sci. Eng. B* **167**, 153 (2010).
- 356 [6] R. Jothiramalingam and M. K. Wang, *J. Porous Mater.* **17**, 677 (2010).
- 357 [7] C. Kittel, *Introduction to Solid State Physics* (Wiley, New York, 1986).
- 358 [8] G. A. Slack, *J. Appl. Phys.* **31**, 1571 (1960).
- 359 [9] H. Shaked, J. Faber Jr., and R. L. Hitterman, *Phys. Rev. B* **38**, 11901 (1988).

- 360 [10] R. N. Iskenderov, I. A. Drabkin, L. T. Emel'yanova, and Y. M. Ksendzov, *Fiz. Tverd. Tela*  
361 (Leningrad) **10**, 2573 (1968).
- 362 [11] J. van Elp, R. H. Potze, H. Eskes, R. Berger, and G. A. Sawatzky, *Phys. Rev. B* **44**, 1530  
363 (1991).
- 364 [12] W. C. Mackrodt, N. M. Harrison, V. R. Saunders, N. L. Allan, M. D. Towler, E. Apra, and  
365 R. Dovesi, *Philos. Mag. A* **68**, 653 (1993).
- 366 [13] M. D. Towler, N. L. Allan, N. M. Harrison, V. R. Saunders, W. C. Mackrodt, and E. Apra,  
367 *Phys. Rev. B* **50**, 5041 (1994).
- 368 [14] S. Massidda, M. Posternak, A. Baldereschi, and R. Resta, *Phys. Rev. Lett.* **82**, 430 (1999).
- 369 [15] X. Feng, *Phys. Rev. B* **69**, 155107 (2004).
- 370 [16] C. Franchini, V. Bayer, R. Podloucky, J. Paier, and G. Kresse, *Phys. Rev. B* **72**, 045132  
371 (2005).
- 372 [17] A. Schron and F. Bechstedt, *Phys. Rev. B* **82**, 165109 (2010).
- 373 [18] P. Dufek, P. Blaha, V. Sliwko, and K. Schwarz, *Phys. Rev. B* **49**, 10170 (1994).
- 374 [19] J. Hugel and M. Kamal, *Solid State Commun.* **100**, 457 (1996).
- 375 [20] J. E. Pask, D. J. Singh, I. I. Mazin, C. S. Hellberg, and J. Kortus, *Phys. Rev. B* **64**, 024403  
376 (2001).
- 377 [21] C. Franchini, R. Podloucky, J. Paier, M. Marsman, and G. Kresse, *Phys. Rev. B* **75**, 195128  
378 (2007).
- 379 [22] A. Schron, C. Rodl, and F. Bechstedt, *Phys. Rev. B* **86**, 115134 (2012).
- 380 [23] A. Schron, M. Granovskij, and F. Bechstedt, *J. Phys.: Condens. Matter* **25**, 094006 (2013).
- 381 [24] H. Jiang, R. I. Gomez-Abal, P. Rinke, and M. Scheffler, *Phys. Rev. B* **82**, 045108 (2010).
- 382 [25] E. Engel and R. N. Schmid, *Phys. Rev. Lett.* **103**, 036404 (2009).
- 383 [26] J. B. Goodenough and A. L. Loeb, *Phys. Rev. Lett.* **98**, 391 (1955).
- 384 [27] A. S. Borovik-Romanov and M. P. Orlova, *Soviet Phys. JETP* **5**, 1023 (1957).
- 385 [28] Y. Yafet and C. Kittel, *Phys. Rev. Lett.* **87**, 290 (1952).
- 386 [29] I. S. Jacobs, *J. Phys. Chem. Solids* **11**, 1 (1959).
- 387 [30] K. Dwight and N. Menyuk, *Phys. Rev. Lett.* **119**, 1470 (1960).
- 388 [31] G. Srinivasan and M. S. Seehra, *Phys. Rev. B* **28**, 1 (1983).
- 389 [32] B. Boucher, R. Buhl, and M. Perrin, *J. Appl. Phys.* **42**, 1615 (1971).
- 390 [33] G. B. Jensen and O. V. Nielsen, *J. Phys. C: Solid State Phys.* **7**, 409 (1974).

- 391 [34] S. Hirai, Y. Goto, A. Wakatsuki, Y. Kamihara, M. Matoba, and W. L. Mao, (2014).
- 392 [35] D. P. Dubal, D. S. Dhawale, R. R. Salunkhe, V. J. Fularim, and C. D. Lokhande, *J. Alloys*  
393 *Compd.* **497**, 166 (2010).
- 394 [36] A. Jha, R. Thapa, and K. K. Chattopadhyay, *Mater. Res. Bull.* **47**, 813 (2012).
- 395 [37] A. Chartier, P. D'Arco, R. Dovesi, and V. R. Saunders, *Phys. Rev. B* **60**, 14042 (1999).
- 396 [38] Q. Liu, Y. Li, Z. Hu, D. Mao, C. Chang, and F. Huang, *Electrochim. Acta* **53**, 7298 (2008).
- 397 [39] N. N. Tusar, D. Maucec, M. Rangus, I. Arcon, M. Mozaj, M. Cotman, A. Pintar, and  
398 V. Kaucic, *Adv. Funct. Mater.* **22**, 820 (2012).
- 399 [40] M. Baldi, V. S. Escribano, J. M. G. Amores, F. Milella, and G. Busca, *Appl. Catal. B:*  
400 *Environ.* **17**, L175 (1998).
- 401 [41] S. Geller, *Acta Cryst.* **27**, 821 (1970).
- 402 [42] E. G. King, *J. Am. Chem. Soc.* **76**, 3289 (1954).
- 403 [43] J. Cable, M. Wilkinson, E. Woolan, and W. Koehler, *Phys. Prog. Rep.*, 43 (1957).
- 404 [44] R. R. Chevalier, G. Roullet, and E. F. Bertaut, *Solid State Commun.* **5**, 7 (1967).
- 405 [45] R. W. Grant, S. Geller, J. A. Cafe, and G. P. Espinosa, *Phys. Rev. Lett.* **175**, 686 (1968).
- 406 [46] S. Geller and G. P. Espinosa, *Phys. Rev. B* **1**, 3763 (1970).
- 407 [47] M. Regulski, R. Przenioslo, I. Sosnowska, D. Hohlwein, and R. Schneider, *J. Alloys Compd.*  
408 **362**, 236 (2004).
- 409 [48] E. Cockayne, I. Levin, H. Wu, and A. Llobet, *Phys. Rev. B* **87**, 184413 (2013).
- 410 [49] Q.-u.-a. Javed, W. Feng-Ping, M. Y. Rafique, A. M. Toufiq, and M. Z. Iqbal, *Chin. Phys. B*  
411 **21**, 117311 (2012).
- 412 [50] J. M. Tarascon and D. Guyomard, *Electrochim. Acta* **38**, 1221 (1993).
- 413 [51] G. Pistoia and G. Wang, *Solid State Ionics* **66**, 135 (1993).
- 414 [52] H. Huang and P. G. Bruce, *J. Power Sources* **54**, 52 (1995).
- 415 [53] A. R. Armstrong and P. G. Bruce, *Nature* **381**, 499 (1996).
- 416 [54] X. Wang and Y. Li, *J. Am. Chem. Soc.* **124**, 2880 (2002).
- 417 [55] W. Tang, X. Yang, Z. Liu, and K. Ooi, *J. Mater. Chem.* **13**, 2989 (2003).
- 418 [56] F. Cheng, J. Zhao, W. Song, C. Li, H. Ma, J. Chen, and P. Shen, *Inorg. Chem.* **45**, 2038  
419 (2006).
- 420 [57] J.-Y. Luo, J.-J. Zhang, and Y.-Y. Xia, *Chem. Mater.* **18**, 5618 (2006).
- 421 [58] F. Jiao and P. G. Bruce, *Adv. Mater.* **19**, 657 (2007).

- 422 [59] V. Mathew, J. Lim, J. Kang, J. Gim, A. K. Rai, and J. Kim, *Electrochem. Commun.* **13**,  
423 730 (2011).
- 424 [60] D. Wang, L.-M. Liu, S.-J. Zhao, B.-H. Li, H. Liu, and X.-F. Lang, *Phys. Chem. Chem.*  
425 *Phys.* **15**, 9075 (2013).
- 426 [61] A. Debart, A. J. Paterson, J. Bao, and P. G. Bruce, *Angew. Chem. Int. Ed.* **47**, 4521 (2008).
- 427 [62] A. K. Thapa, Y. Hidaka, H. Hagiwara, S. Ida, and T. Ishihara, *J. Electrochem. Soc.* **158**,  
428 A1483 (2011).
- 429 [63] M. Toupin, T. Brousse, and D. Belanger, *Chem. Mater.* **14**, 3946 (2002).
- 430 [64] V. Subramanian, H. Zhu, R. Vajtai, P. M. Ajayan, and B. Wei, *J. Phys. Chem. B* **109**,  
431 20207 (2005).
- 432 [65] S. Devaraj and N. Munichandraiah, *J. Phys. Chem. C* **112**, 4406 (2008).
- 433 [66] H. Zhang, G. Cao, Z. Wang, Y. Yang, Z. Shi, and Z. Gu, *Nano Lett.* **8**, 2664 (2008).
- 434 [67] X. Lang, A. Hirata, T. Fujita, and M. Chen, *Nat. Nanotechnol.* **6**, 232 (2011).
- 435 [68] J. Zang and X. Li, *J. Mater. Chem.* **21**, 10965 (2011).
- 436 [69] L. Espinal, W. Wong-Ng, J. A. Kaduk, A. J. Allen, C. R. Snyder, C. Chiu, D. W. Siderius,  
437 L. Li, E. Cockayne, A. E. Espinal, and S. L. Suib, *J. Am. Chem. Soc.* **134**, 7944 (2012).
- 438 [70] R. Andreozzi, A. Insola, V. Caprio, R. Marotta, and V. Tufano, *Appl. Catal. A: General*  
439 **138**, 75 (1996).
- 440 [71] F. H. B. Lima, M. L. Calegario, and E. A. Ticianelli, *Electrochim. Acta* **52**, 3732 (2007).
- 441 [72] H. Sato and T. Enoki, *Phys. Rev. B* **61**, 3563 (2000).
- 442 [73] X. L. Yu, S. X. Wu, Y. J. Liu, and S. W. Li, *Solid State Commun.* **146**, 166 (2008).
- 443 [74] W. C. Mackrodt and E.-A. Williamson, *J. Chem. Soc., Faraday Trans.* **93**, 3295 (1997).
- 444 [75] E. Cockayne and L. Li, *Chem. Phys. Lett.* **544**, 53 (2012).
- 445 [76] D. A. Tompsett, D. S. Middlemiss, and M. S. Islam, *Phys. Rev. B* **86**, 205126 (2012).
- 446 [77] A. Yoshimori, *J. Phys. Soc. Jpn.* **14**, 807 (1959).
- 447 [78] M. Zhuang and J. W. Halley, *Phys. Rev. B* **64**, 024413 (2001).
- 448 [79] S. L. Dudarev, G. A. Botton, S. Y. Savrasov, C. J. Humphreys, and A. P. Sutton, *Phys.*  
449 *Rev. B* **57**, 1505 (1998).
- 450 [80] V. I. Anisimov, J. Zaanen, and O. K. Anderson, *Phys. Rev. B* **44**, 943 (1991).
- 451 [81] A. I. Liechtenstein, V. I. Anisimov, and J. Zaanen, *Phys. Rev. B* **52**, R5467 (1995).
- 452 [82] B. Himmetoglu, R. M. Wentzcovitch, and M. Cococcioni, *Phys. Rev. B* **84**, 115108 (2011).

- 453 [83] A. D. Becke, J. Chem. Phys. **98**, 1372 (1993).
- 454 [84] E. Bousquet and N. Spaldin, Phys. Rev. B **82**, 220402 (2010).
- 455 [85] J. P. Perdew, A. Ruzsinszky, G. I. Csonka, O. A. Vydrov, G. E. Scuseria, L. A. Constantin,  
456 X. Zhou, and K. Burke, Phys. Rev. Lett. **100**, 136406 (2008).
- 457 [86] Y.-C. Wang, Z.-H. Chen, and H. Jiang, J. Chem. Phys. **144**, 144106 (2016).
- 458 [87] P. Giannozzi, S. Baroni, N. Bonini, M. Calandra, R. Car, C. Cavazzoni, D. Ceresoli, G. L.  
459 Chiarotti, M. Cococcioni, I. Dabo, A. Dal Corso, S. de Gironcoli, S. Fabris, G. Fratesi,  
460 R. Gebauer, U. Gerstmann, C. Gougoussis, A. Kokalj, M. Lazzeri, L. Martin-Samos,  
461 N. Marzari, F. Mauri, R. Mazzarello, S. Paolini, A. Pasquarello, L. Paulatto, C. Sbraccia,  
462 S. Scandolo, G. Sciauzero, A. P. Seitsonen, A. Smogunov, P. Umari, and R. M. Wentzcovitch,  
463 J. Phys.: Condens. Matter **21**, 395502 (2009).
- 464 [88] M. Cococcioni and S. de Gironcoli, Phys. Rev. B **71**, 035105 (2005).
- 465 [89] A. M. Rappe, K. M. Rabe, E. Kaxiras, and J. D. Joannopoulos, Phys. Rev. B **41**, 1227  
466 (1990).
- 467 [90] N. J. Ramer and A. M. Rappe, Phys. Rev. B **59**, 12471 (1999).
- 468 [91] <http://opium.sourceforge.net>.
- 469 [92] S. G. Louie, S. Froyen, and M. L. Cohen, Phys. Rev. B **26**, 1738 (1982).
- 470 [93] M. Fuchs and M. Scheffler, Comput. Phys. Commun. **119**, 67 (1999).
- 471 [94] D. Porezag, M. R. Pederson, and A. Y. Liu, Phys. Rev. B **60**, 14132 (1999).
- 472 [95] H. J. Monkhorst and J. D. Pack, Phys. Rev. B **13**, 5188 (1976).
- 473 [96] S. Sasaki, K. Fujino, Y. Takeuchi, and R. Sadanaga, Acta Cryst. **A36**, 904 (1980).
- 474 [97] A. K. Cheetham and D. A. O. Hope, Phys. Rev. B **27**, 6964 (1983).
- 475 [98] R. G. Wyckoff, *Crystal Structures* (Wiley, New York, 1963).
- 476 [99] N. Ohama and Y. Hamaguchi, J. Phys. Soc. Jpn. **30**, 1311 (1971).
- 477 [100] M. Regulski, R. Przenioslo, and I. Sosnowska, Phys. Rev. B **68**, 172401 (2003).
- 478 [101] C. Rodl, F. Fuchs, J. Furthmuller, and F. Bechstedt, Phys. Rev. B **79**, 235114 (2009).
- 479 [102] B. Mehdaoui, O. Pena, M. Bahout, A. B. Antunes, and G. Martinez, Bol. Soc. Esp. Ceram.  
480 V. **47**, 143 (2008).
- 481 [103] J.-H. Chung, J.-H. Kim, S.-H. Lee, T. J. Sato, T. Suzuki, M. Katsumura, and T. Katsufuji,  
482 Phys. Rev. B **77**, 054412 (2008).
- 483 [104] B. Chardon and F. Vigneron, J. Magn. Magn. Mater. **58**, 128 (1986).

- 484 [105] A. Kuriki, Y. Moritomo, S. Xu, K. Ohoyama, K. Kato, and A. Nakamura, J. Phys. Soc.  
485 Jpn. **72**, 458 (2003).
- 486 [106] E. Jo, K. An, J. H. Shim, C. Kim, and S. Lee, Phys. Rev. B **84**, 174423 (2011).
- 487 [107] E. O. Wollan and W. C. Koehler, Phys. Rev. **100**, 545 (1955).
- 488 [108] R. G. Wyckoff, *Crystal Structures*, Vol. 1 (Interscience, New York, 1960).
- 489 [109] A. A. Bolzan, C. Fong, B. J. Kennedy, and C. J. Howard, Aust. J. Chem. **46**, 939 (1993).